

A Novel Convolution and Attention Mechanism-based Model for 6D Object Pose Estimation

Alexander Du¹
California Institute of Technology

Xiujin Liu¹
University of Michigan

Abstract—This paper proposes PoseLecTr, a graph-based encoder-decoder framework that integrates a novel Legendre convolution with attention mechanisms for six-degree-of-freedom (6-DOF) object pose estimation from monocular RGB images. Conventional learning-based approaches predominantly rely on grid-structured convolutions, which can limit their ability to model higher-order and long-range dependencies among image features, especially in cluttered or occluded scenes. PoseLecTr addresses this limitation by constructing a graph representation from image features, where spatial relationships are explicitly modeled through graph connectivity. The proposed framework incorporates a Legendre convolution layer to improve numerical stability in graph convolution, together with spatial-attention and self-attention distillation to enhance feature selection.

Experiments conducted on the LINEMOD [1], Occluded LINEMOD [2], and YCB-VIDEO datasets [3] demonstrate that our method achieves competitive performance and shows consistent improvements across a wide range of objects and scene complexities.

Index Terms—6D Pose Estimation, Legendre Convolution, GNN, Spatial Attention

I. INTRODUCTION

Recognizing objects and estimating their 6-DOF pose $(x, y, z, \theta, \psi, \phi)$ in real-world environments is a fundamental challenge in computer vision and robotic perception, with broad applications in autonomous driving [4], augmented reality [5], and industrial automation [6]. Traditional approaches which rely on matching feature points and Perspective-n-Point (PnP) typically require clear textures, and lack effectiveness for texture-less objects. More recent methods incorporate deep learning to analyze large datasets and extract robust features from images. However, these approaches often struggle to capture dependencies among extracted features, partly due to the inherent limitations of grid-based convolutional architectures. To address these limitations, we propose PoseLecTr, a graph-based encoder-decoder architecture that encodes image features as nodes and utilizes an adjacency matrix to model their relationships. This design leverages a graph neural network (GNN) to capture both local and global feature dependencies, while spatial-attention, self-attention distillation, and a Legendre convolution method further refine accuracy.

Our key contributions are as follows:

a) Graph-Based Representation: We introduce a novel graph-based representation for image features, enabling more flexible and expressive feature interactions compared to traditional grid-based CNNs.

b) Legendre Convolution: We propose a novel Legendre convolution layer, which significantly improves numerical stability compared to standard graph convolutional layers.

c) Spatial-Attention and Self-Attention Distillation: We incorporate advanced spatial-attention and self-attention distillation mechanisms to enhance feature extraction and focus on critical spatial information.

II. RELATED WORKS

Accurate 6D object pose estimation determines both the orientation and position of an object in three-dimensional space. Non-learning approaches have relied on matching feature points between 3D model projections and images [7]–[9], or on offline template databases for pose retrieval [10], [11]. The advancement of deep learning has significantly accelerated the progress of 6-DOF pose estimation, enabling accurate pose prediction from a single RGB image. Convolutional neural networks (CNNs)-based methods such as [3], [12], [13] show improved performance for 3D position and rotation estimation, but require large amounts of labeled data. More recent work [14] eliminates the need for large amounts of labeled data and enables 6D pose estimation on novel objects. While grid-based convolutional models may overlook high-level feature dependencies, recent work has increasingly focused on graph-based neural networks [15]–[17], which can capture complex relationships through node-grid representations and offer a promising avenue for advancing 6D pose estimation.

Several challenges remain. Existing 6-DOF pose estimation methods still primarily rely on grid-based convolutional neural networks, which are effective for extracting features from images. However, traditional 2D convolution can only capture features from neighboring pixels and is limited in its ability to capture the correlation between different features at higher levels of abstraction. Graph-based representations offer a significant advantage due to their flexibility. Graphs can be constructed based on semantic similarity rather than just spatial proximity. Although graph-based neural networks have shown promise, several challenges remain in effectively

¹These authors contributed equally to this work

applying graph-based models to 6-DOF pose estimation. In this work, we developed a graph-based encoder-decoder architecture with a novel Legendre convolutional layer with attention mechanisms to address the challenges above and to improve accuracy for pose estimation.

III. METHODOLOGY

A. Architecture

Fig. 1 depicts the structure of PoseLecTr. PoseLecTr has an encoder-decoder structure. Before the encoder, ResNet-50 [18] is used as the backbone to extract image features. The encoder, which serves as a feature aggregation neck, consists of spatial-attention blocks to capture complex spatial dependencies on 3D objects, and a graph neural network block with Legendre convolution blocks. The decoder layer outputs the final 6D pose estimation.

B. Input and Output

The goal of PoseLecTr is to estimate the homogeneous transformation matrix of camera pose related to object pose. The inputs for the PoseLecTr are monocular RGB images of size $H \times W \times 3$, where H and W are the height and width of the images. The images contain objects with specific camera poses. The output of the PoseLecTr is a predicted 12×1 vector, where the first 9 elements are reshaped to a 3×3 rotation matrix, and the remaining 3 elements represent the translation vector.

C. Graph Neural Network

A graph structure is used to organize spatial features of 3D objects extracted from images. Formally, the graph is denoted as $G(V, E, A)$, where $V = \{v_1, v_2, \dots, v_N\}$ denotes a set of nodes N corresponding to feature maps of extraction layers; $E \subseteq V \times V$ is a set of edges representing the connections between nodes; and $A \in \mathbb{R}^{N \times N}$ is a real-number adjacency matrix constructed based on the four-neighbors of feature maps, capturing the relational information between different regions of the images.

D. Legendre Convolution Layer

Legendre polynomials offer the following advantageous mathematical properties for functional representation. [19]

a) *Orthogonality*: Polynomials of different orders are mutually orthogonal under the standard inner product on $[-1, 1]$, allowing expansion coefficients to be computed independently and simplifying the fitting process.

b) *Numerical Stability*: They exhibit strong numerical stability, which helps suppress oscillatory artifacts such as Runge's phenomenon [20] when using high-order approximations.

c) *Recursion*: Legendre polynomials satisfy a simple recursive formulation, enabling efficient construction of higher-order terms.

For these reasons, we integrate Legendre polynomials into our proposed Legendre Convolution Layer to achieve stable, efficient, and mathematically well-structured feature modeling.

The Legendre convolution layer includes the spatial graph Laplacian embedding for encoding the spatial relationships within the feature maps. To characterize the interconnections between nodes in the graph, we utilize the regularized Laplacian matrix denoted as $L = I - D^{-0.5}AD^{-0.5}$, where A represents the adjacency matrix, I is the identity matrix, and D is the matrix of node degrees in diagonal form. As L is a symmetric positive semi-definite matrix, its eigenvectors are orthogonal in pairs, and the eigenvalues are distinct and non-negative. Therefore, L can be simplified to the form of $L = U\Delta U^T$, where U is a matrix composed of eigenvectors and Δ is a matrix composed of eigenvalues. In our model, the output of Legendre convolution layer is defined as $Y_{output} = \sigma(Ug_{\theta}(\Delta)U^T X_{input})$, where $\sigma(\cdot)$ denotes the activation function, and θ is the parameter value for iterative updates. Here, $g_{\theta}(\Delta)$ signifies the convolution kernel operating on a graph.

Legendre polynomials can be written recursively as

$$\begin{aligned} P_0 &= 1 \\ P_1(x) &= x(n+1) \\ P_{n+1}(x) &= (2n+1)xP_n(x) - nP_{n-1}(x) \\ n &= 1, 2, 3, \dots \end{aligned} \quad (1)$$

In this work, Legendre polynomials are used to approximate the convolution kernel. Legendre polynomials are defined as

$$\begin{aligned} P_0(x) &= 1 \\ P_n(x) &= \frac{1}{2^n n!} \frac{d^n}{dx^n} [(x^2 - 1)^n] \\ n &= 1, 2, 3, \dots \end{aligned} \quad (2)$$

We write the Legendre convolution block as

$$\begin{aligned} g_{\theta}(\Delta) &= \text{Concat}(\text{Matmul}(\alpha_i P_i(\tilde{\Delta}), x)) \\ i &= 0, 1, \dots, k \end{aligned} \quad (3)$$

E. Spatial Feature Self-Attention

A spatial feature self-attention layer is used to capture spatial features of 3D objects from monocular RGB images for more accurate 6-DOF object pose estimation. Let $\mathbb{X} = (X_1, X_2, \dots, X_T) \subset \mathbb{R}^{T \times N \times D}$ denote the input images, where T represents number of images, N represents number of features extracted from one image, and D represents the feature dimension. The query, key, and value matrices of self-attention operations can be represented as:

$$q^{(i)} = W_q x^{(i)}, k^{(i)} = W_k x^{(i)}, v^{(i)} = W_v x^{(i)} \text{ for } i \in [1, T], \quad (4)$$

where $W_q, W_k, W_v \in \mathbb{R}^{d \times d'}$ are learnable parameters and d' is the dimension of the query, key, and value matrices. The self-attention mechanism, SA , can be expressed as [21]:

$$SA(q, k, v) = \text{Softmax}\left(\frac{qk^T}{\sqrt{d}}\right)v. \quad (5)$$

The spatial dependencies between nodes are different in different X_i . The key to the attention mechanism is the mapping function, which encodes the relative importance of

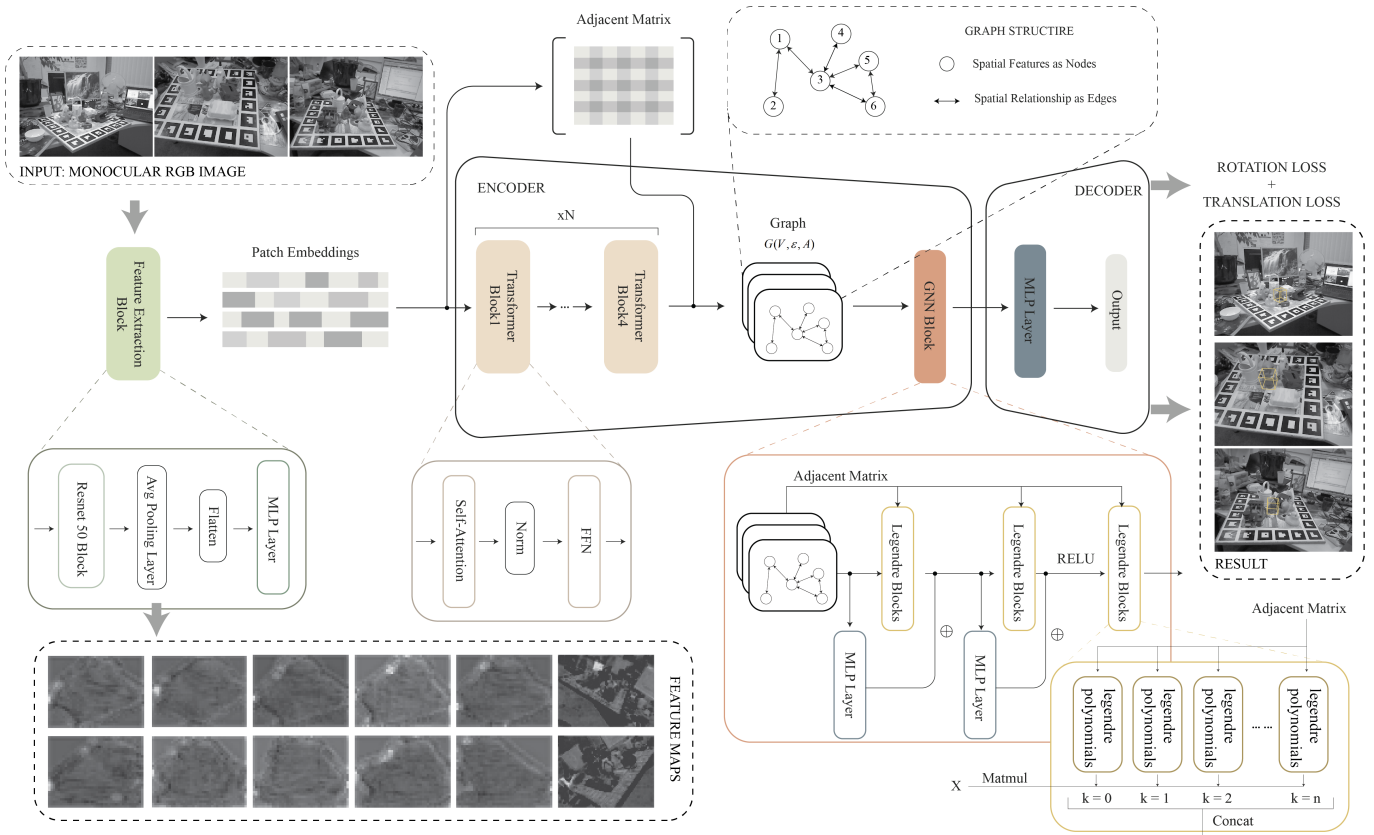


Fig. 1. The architecture of PoseLecTr

the input elements, mapping the values to probabilities. The commonly used softmax function generates dense attention. Note that in the task of 6-DOF pose estimation, the distribution of feature relevance can be highly imbalanced across different regions of the image. Therefore, we introduce a new spatial feature attention module, written as

$$SFA(q, k, v) = \text{Sparsemax}\left(\frac{qk^T}{\sqrt{d}}\right)v. \quad (6)$$

In contrast to the Softmax function in Equation 5, the Sparsemax function generates sparse probability distributions. Sparsemax has the ability to selectively emphasize the most significant features while disregarding less relevant ones, thus offering clearer decision boundaries [22]. Furthermore, when handling complex image data for 6-DOF pose estimation, Sparsemax is better at handling the long-tail effects, ensuring the model focuses on the most critical spatial features.

F. Loss Function

In PoseLecTr, the total loss function consists of two components, rotation matrix loss and translation vector loss. These two losses evaluate both the orientation and translation of the predicted poses relative to the ground truth. The first term of our loss function measures the discrepancy between the predicted rotation matrix \hat{R} and the ground-truth rotation matrix R . We use the Frobenius norm of the difference

between these two matrices, which captures the magnitude differences between them. The loss function is defined as

$$L_R = \frac{1}{n} \sum_{i=1}^n \left\| \hat{R}_i - R_i \right\|_F^2, \quad (7)$$

where $\|\cdot\|_F$ denotes the Frobenius norm.

The second term is the Mean Squared Error (MSE) between the predicted translation vector \hat{t} and the ground truth translation vector t . The translation loss function is given by

$$L_t = \frac{1}{n} \sum_{i=1}^n \left\| \hat{t}_i - t_i \right\|_F^2, \quad (8)$$

where \hat{t}_i represents the predicted translation vector and t_i is the corresponding ground truth translation vector.

The final loss function is a weighted sum of the rotation loss function and translation loss function. The total loss function is defined as

$$L = \eta_1 L_R + \eta_2 L_t, \quad (9)$$

where η_1 and η_2 are weighting parameters for each loss term.

IV. EXPERIMENTS

A. Datasets

We evaluate our method on three widely recognized benchmarks: LINEMOD dataset [1], YCB-Video dataset [3] and Occluded LINEMOD dataset [2]. The LINEMOD dataset consists of 15 registered video sequences, each containing over

TABLE I
QUANTITATIVE EVALUATION OF DIFFERENT 6D POSE ESTIMATION BASELINES ON LINEMOD DATASET.

Object	PoseCNN [3]		DenseFusion [23]		PVNet [12]		PoseRBPF [24]		DeepIM [13]		GC-Pose [25]		G2LNet [26]		TransPose [27]		Ours	
	ADDS	ADD	ADDS	ADD	ADDS	ADD	ADDS	ADD	ADDS	ADD	ADDS	ADD	ADDS	ADD	ADDS	ADD	ADDS	ADD
ape	90.4	90.3	96.6	95.7	92.4	91.3	89.1	88.4	91.0	90.8	93.4	92.8	95.2	94.5	96.0	95.8	98.9	98.0
benchvise	89.8	89.6	98.0	97.7	89.2	88.6	86.7	86.0	90.8	90.4	94.1	93.0	93.4	92.9	96.6	96.4	99.6	99.4
cam	96.6	96.2	99.8	98.7	92.6	91.7	91.7	91.6	94.3	93.2	94.4	94.1	97.3	96.6	97.3	96.3	98.4	98.3
can	89.8	89.7	96.1	95.4	90.8	90.1	89.3	88.2	93.4	92.3	92.5	92.4	94.4	94.0	96.4	95.6	100	99.9
cat	91.0	89.9	97.8	97.1	89.9	89.7	85.7	85.3	91.1	91.1	93.4	92.7	94.6	93.5	96.7	96.6	99.4	98.8
driller	96.9	96.2	100	99.2	92.7	91.6	92.2	91.6	95.5	94.3	96.0	95.4	96.9	95.9	97.8	97.0	99.1	98.8
duck	91.5	90.9	96.0	95.6	90.5	89.9	88.3	88.1	92.4	92.1	93.3	92.2	94.3	94.1	95.4	94.9	100	99.3
eggbox	94.5	93.9	96.9	96.8	92.0	91.4	90.2	90.0	93.1	92.1	95.5	94.3	96.1	95.5	98.1	97.3	99.5	98.9
glue	79.2	78.5	87.8	87.6	80.8	80.2	79.4	78.7	83.5	82.5	85.8	85.1	86.6	85.5	88.8	87.7	91.3	92.7
holepuncher	82.2	82.1	100	99.6	85.6	85.6	83.5	82.7	85.2	85.1	87.4	86.9	89.1	88.4	91.0	90.1	94.7	93.7
iron	91.7	90.9	100	99.3	95.0	94.1	91.1	91.0	94.2	93.4	95.9	95.5	97.8	97.1	98.4	98.3	99.3	99.2
lamp	82.8	82.2	79.4	78.2	83.1	82.0	80.5	79.6	83.6	82.6	85.9	85.3	86.6	85.6	88.6	87.8	91.1	91.1
phone	83.4	83.3	96.7	96.5	86.0	85.2	83.8	83.5	87.6	87.1	90.1	89.2	90.9	90.5	93.1	92.2	99.6	98.6
MEAN	89.2	88.7	95.8	95.2	89.3	88.6	87.0	86.5	90.4	89.8	92.1	91.5	93.3	92.6	94.9	94.3	97.8	97.4

TABLE II
QUANTITATIVE EVALUATION OF DIFFERENT 6D POSE ESTIMATION BASELINES ON YCB-VIDEO DATASET.

Object	PoseCNN [3]		DenseFusion [23]		PVNet [12]		PoseRBPF [24]		DeepIM [13]		GC-Pose [25]		G2LNet [26]		TransPose [27]		Ours	
	ADDS	ADD	ADDS	ADD	ADDS	ADD	ADDS	ADD	ADDS	ADD	ADDS	ADD	ADDS	ADD	ADDS	ADD	ADDS	ADD
002_master_chef_can	89.0	85.3	93.9	92.2	89.3	87.1	86.5	84.4	90.2	89.6	91.5	89.6	92.7	89.0	94.0	93.7	96.4	93.9
003_cracker_box	88.5	86.6	96.5	94.5	87.8	85.2	85.0	83.6	89.9	87.2	91.0	88.2	92.5	89.1	94.7	93.2	97.8	97.1
004_sugar_box	94.3	91.9	97.6	95.7	91.2	87.3	89.7	87.8	92.3	91.2	93.5	92.0	94.8	91.7	96.0	95.8	97.5	95.5
005_tomato_soup_can	89.1	87.3	95.0	94.5	88.9	87.8	86.8	83.6	90.7	89.9	91.9	90.1	93.2	90.0	94.5	93.2	98.5	96.7
006_mustard_bottle	92.0	91.6	95.8	91.9	90.5	89.2	88.6	86.1	91.8	90.3	93.0	92.3	94.2	92.6	95.5	95.0	97.3	96.3
007_tuna_fish_can	78.0	77.1	86.5	83.0	79.3	75.7	77.5	75.2	81.8	78.6	83.2	81.0	84.5	82.7	85.8	85.6	91.2	88.0
008_pudding_box	81.4	77.5	97.9	96.6	83.7	83.2	80.9	79.3	84.2	81.7	85.6	85.1	87.1	85.2	89.3	87.3	91.8	89.8
009_gelatin_box	90.4	90.0	97.8	94.9	92.1	88.6	89.8	89.7	93.0	91.0	94.2	93.0	95.6	93.2	96.7	93.7	98.7	95.8
010_potted_meat_can	81.7	77.9	77.8	74.4	80.3	78.9	78.2	76.9	82.1	79.9	83.5	80.2	84.9	83.5	86.3	82.6	90.2	88.2
011_banana	82.6	80.1	94.9	93.5	84.5	81.1	83.2	79.6	86.5	84.5	87.8	84.4	89.1	88.2	91.3	88.1	96.9	95.2
MEAN	86.7	84.5	93.4	91.1	86.7	84.4	84.6	82.6	88.3	86.4	89.5	87.6	90.1	88.5	92.4	90.8	95.6	93.6

TABLE III
QUANTITATIVE EVALUATION OF DIFFERENT 6D POSE ESTIMATION BASELINES ON OCCLUDED LINEMOD DATASET.

Object	PoseCNN [3]		DenseFusion [23]		PVNet [12]		PoseRBPF [24]		DeepIM [13]		GC-Pose [25]		G2LNet [26]		TransPose [27]		Ours	
	ADDS	ADD	ADDS	ADD	ADDS	ADD	ADDS	ADD	ADDS	ADD	ADDS	ADD	ADDS	ADD	ADDS	ADD	ADDS	ADD
ape	86.8	85.5	91.6	90.0	89.0	87.9	84.1	82.9	88.1	86.4	90.6	89.5	91.2	89.8	93.1	91.8	93.7	92.3
can	85.5	83.9	93.2	91.9	86.2	85.0	83.3	82.1	89.1	87.8	89.8	88.5	91.8	90.5	92.3	90.6	95.5	94.3
cat	91.6	89.9	96.1	94.7	90.5	88.9	89.3	88.0	90.4	89.4	91.9	90.2	91.7	90.1	94.4	92.9	95.5	93.7
driller	87.3	85.6	94.6	93.3	86.5	84.9	86.2	84.6	89.5	87.9	90.7	89.2	91.8	90.2	94.2	92.6	94.3	92.9
duck	86.2	84.4	93.9	92.3	87.3	85.6	83.6	82.1	89.8	88.6	90.3	88.9	90.4	89.1	92.8	91.5	93.8	92.5
eggbox	93.2	92.2	96.9	95.4	89.0	87.9	88.5	87.3	90.8	89.1	90.9	89.2	92.8	91.8	93.6	92.4	95.2	93.6
glue	87.6	86.4	92.6	91.0	87.9	86.5	83.7	82.6	88.7	87.1	90.6	89.4	91.5	89.9	92.5	91.5	92.8	91.4
holepuncher	91.0	89.8	93.6	92.6	89.2	87.9	87.6	86.4	90.4	89.2	91.5	90.3	92.6	90.8	93.5	92.3	95.0	93.8
MEAN	88.7	87.2	94.1	92.7	88.2	86.8	85.8	84.5	89.6	88.2	90.8	89.4	91.7	90.3	93.3	92.0	94.5	93.1

1100 frames. These sequences feature 15 different texture-less household objects, captured in varying poses and lighting conditions. The YCB-Video dataset contains 92 real-world video sequences featuring 21 different objects from the YCB object set, including items such as power drills, cups, and bananas. The Occluded LINEMOD dataset introduces significant occlusion and clutter, facilitating robust testing of algorithm resilience under partial visibility.

B. Comparison Methods

We compared our PoseLecTr to the following eight baseline models that fall into three categories:

a) *CNN-Based Models*: PoseCNN [3] and DenseFusion [23] are benchmark baselines for integrating RGB and depth data to achieve accurate 6-DOF pose estimations. PoseCNN focuses on predicting 3D translation and rotation directly from RGB images, while DenseFusion fuses dense pixel-wise information from both RGB and depth maps. PVNet [12] approaches pose estimation by regressing 2D keypoints from the image, followed by a PnP algorithm to compute the pose, ensuring precision through keypoint localization. PoseRBPF [24] combines recurrent neural networks and particle filters to handle temporal dynamics in pose estimation, making it robust against occlusions and other temporal inconsistencies.

DeepIM [13] iteratively refines an initial pose estimate by aligning rendered and observed images, providing a feedback loop that improves the pose estimation accuracy over several iterations.

b) *GNN-Based Models*: GC-Pose [25] utilizes graph convolutional networks (GCN) to model spatial relationships between object parts as a graph, extracting features from RGB images to capture the geometric structure of the object. G2LNet [26] Employs a GNN to learn spatial relationships between keypoints, using these to predict the 6-DOF pose of the object.

c) *Self-Attention-Based Models*: TransPose [27] adopts a transformer-based architecture to model long-range dependencies in image data, leveraging self-attention mechanisms to focus on image regions most relevant to 6D pose prediction.

C. Implementation Details

Our proposed methods are trained using the Adam optimizer, with an initial learning rate of $1e-4$, which is reduced by half after each epoch. The training process spans 8 epochs, incorporating early stopping to prevent overfitting. All baseline methods are configured according to their recommended settings, using a batch size of 32.

All experiments were carried out with an NVIDIA GeForce 4080 GPU and 64GB of RAM. The code was implemented with Ubuntu 18.04, PyTorch 1.16.10 and Python 3.9.0.

D. Evaluation Metrics

Two metrics are used to measure pose prediction performance, the Average Distance Deviation (ADD) and Average Distance Deviation with Symmetry (ADD-S), written as

$$ADD = \frac{1}{m} \sum_{x \in M} \left\| (Rx + t) - (\hat{R}x + \hat{t}) \right\|. \quad (10)$$

$$ADD_S = \frac{1}{m} \sum_{x_1 \in M} \min_{x_2 \in M} \left\| (Rx_1 + t) - (\hat{R}x_2 + \hat{t}) \right\|. \quad (11)$$

The ADD metric quantifies the accuracy of the predicted attitude by measuring the mean Euclidean distance between the corresponding three-dimensional points of the model. Similarly, for symmetric objects, instead of calculating point-to-point distance, ADD-S measures the average minimum distance between each transformation point in the predicted attitude and the nearest point on the model transformed by the ground-truth pose. If ADD/ADD-S is less than $0.1 \cdot d$, where d is the maximum measurement of the object, the posture is considered correct.

E. Quantitative Results

Table I, Table II and Table III show the experimental results on the LINEMOD dataset [1], YCB-Video dataset [3], and Occluded LINEMOD dataset [2] respectively.

Specifically, for the YCB-Video dataset, on the object *002_master_chef_can*, PoseLecTr achieves the highest accuracy among the evaluated methods, with 96.4% under ADD-S and 93.9% under ADD metrics. On the object

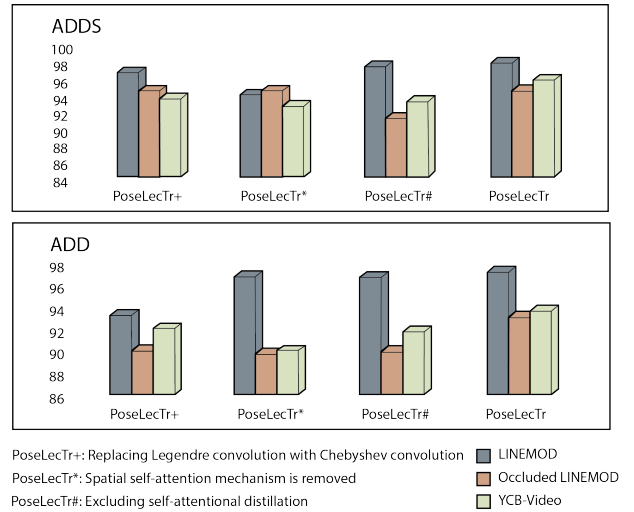


Fig. 2. Visualization of Ablation Studies

003_cracker_box, PoseLecTr records the highest accuracies of 97.8% and 97.1%, while DenseFusion follows with 96.5% and 94.5%. More challenging objects, such as *007_tuna_fish_can*, also highlight PoseLecTr’s advantages, with accuracies of 91.2% and 88%. Considering the overall performance across all frames, PoseLecTr achieves the highest mean accuracy in this comparison for both symmetric and asymmetric objects, scoring 95.6% and 93.6%, indicating consistently strong performance across diverse object categories and evaluation settings.

On the LINEMOD dataset, PoseLecTr achieves mean accuracies of 97.8% and 97.4% under the ADD-S and ADD metrics, respectively, representing the highest results among the evaluated methods.

On the more challenging Occluded LINEMOD dataset, PoseLecTr maintains its robustness by posting mean accuracies of 94.5% and 93.1%.

F. Ablation Studies

As shown in Fig. 2, to further investigate the efficacy of PoseLecTr’s components, we conducted a comparative analysis using several modifications of PoseLecTr.

From the results, we can derive the following insights:

a) *Effect of Graph Convolution Type (PoseLecTr+)*: Replacing Legendre convolution with Chebyshev convolution in PoseLecTr+ results in slightly lower performance across all datasets. On the LINEMOD dataset, accuracy decreases from 99.7% (PoseLecTr) to 96.4%, with similar declines on Occluded LINEMOD (94.34% vs. 95.54%) and YCB-Video (91.56% vs. 93.36%). These results indicate that Legendre convolution provides more effective modeling of both local and global contexts than Chebyshev convolution.

b) *Effects of Spatial Feature Self-Attention (PoseLecTr*)*: When the spatial self-attention mechanism is removed from PoseLecTr*, the accuracy on Occluded LINEMOD (92.54%) and YCB-Video (89.96%) decreases more substantially. This indicates that spatial self-attention is particularly important in handling occlusion and complex scenes. Meanwhile, the

performance on LINEMOD (96.9%) remains relatively stable, suggesting that removing spatial self-attention chiefly affects more challenging datasets where spatial dependencies play a more critical role.

c) *Effects of Self-Attentional Distillation (PoseLecTr#)*:

Excluding self-attentional distillation from PoseLecTr# modules leads to a decline in performance, particularly on LINEMOD (92.64%) and YCB-Video (89.56%). These results indicate that self-focused distillation is essential for handling larger graph sizes and extended data. Without this component, the model’s capacity to manage extensive spatial relationships is diminished, thereby reducing its ability to generalize to more complex environments.

V. CONCLUSION

In this paper, we present PoseLecTr, a novel graph-based framework for 6D object pose estimation from monocular RGB images. By incorporating Legendre convolution and attention mechanisms, PoseLecTr advances accuracy in pose estimation tasks. The introduction of Legendre convolution, with its orthogonality and numerical stability properties, streamlines the convolution process and enables more efficient feature extraction compared to traditional convolution methods. Additionally, the spatial feature self-attention and self-attention distillation modules enhance the model’s ability to focus on critical spatial features, thus improving the robustness and accuracy of pose estimation. Experimental results on benchmark datasets such as LINEMOD [1], Occluded LINEMOD [2] and YCB-Video [3] demonstrate that PoseLecTr achieves competitive performance relative to existing state-of-the-art models, particularly in complex scenes involving textureless, symmetric, or highly occluded objects.

REFERENCES

- [1] Stefan Hinterstoisser, Vincent Lepetit, Slobodan Ilic, Stefan Holzer, Gary Bradski, Kurt Konolige, and Nassir Navab, “Model based training, detection and pose estimation of texture-less 3d objects in heavily cluttered scenes,” in *Computer Vision-ACCV 2012: 11th Asian Conference on Computer Vision, Daejeon, Korea, November 5-9, 2012, Revised Selected Papers, Part I 11*. Springer, 2013, pp. 548–562.
- [2] Eric Brachmann, Alexander Krull, Frank Michel, Stefan Gumhold, Jamie Shotton, and Carsten Rother, “Learning 6d object pose estimation using 3d object coordinates,” in *European conference on computer vision*. Springer, 2014, pp. 536–551.
- [3] Yu Xiang, Tanner Schmidt, Venkatraman Narayanan, and Dieter Fox, “Posecnn: A convolutional neural network for 6d object pose estimation in cluttered scenes,” *arXiv preprint arXiv:1711.00199*, 2017.
- [4] Sabera Hoque, Shuxiang Xu, Ananda Maiti, Yuchen Wei, and Md Yasir Arafat, “Deep learning for 6d pose estimation of objects—a case study for autonomous driving,” *Expert Systems with Applications*, vol. 223, pp. 119838, 2023.
- [5] Mayura Manawadu, Sieun Park, and Soon-Yong Park, “Advancing 6d pose estimation in augmented reality—overcoming projection ambiguity with uncontrolled imagery,” *arXiv preprint arXiv:2403.13434*, 2024.
- [6] Elena Govi, Davide Sapienza, Samuele Toscani, Ivan Cotti, Giorgia Franchini, and Marko Bertogna, “Addressing challenges in industrial pick and place: A deep learning-based 6 degrees-of-freedom pose estimation solution,” *Computers in Industry*, vol. 161, pp. 104130, 2024.
- [7] Vincent Lepetit, Francesc Moreno-Noguer, and Pascal Fua, “EPnP: An accurate O(n) solution to the PnP problem,” *International Journal of Computer Vision*, vol. 81, no. 2, pp. 155–166, 2009.
- [8] Shiqi Li, Chi Xu, and Ming Xie, “A robust o (n) solution to the perspective-n-point problem,” *IEEE Transactions on Pattern Analysis and Machine Intelligence*, vol. 34, no. 7, pp. 1444–1450, 2012.
- [9] Xiujiu Liu, “Gnc-pose: Geometry-aware gnc-pnp for accurate 6d pose estimation,” *arXiv preprint arXiv:2512.06565*, 2025.
- [10] Markus Ulrich, Christian Wiedemann, and Carsten Steger, “Combining scale-space and similarity-based aspect graphs for fast 3d object recognition,” *IEEE transactions on pattern analysis and machine intelligence*, vol. 34, no. 10, pp. 1902–1914, 2011.
- [11] Nadia Payet and Sinisa Todorovic, “From contours to 3d object detection and pose estimation,” in *2011 International Conference on Computer Vision*. IEEE, 2011, pp. 983–990.
- [12] Sida Peng, Yuan Liu, Qixing Huang, Xiaowei Zhou, and Hujun Bao, “Pvnet: Pixel-wise voting network for 6dof pose estimation,” in *Proceedings of the IEEE/CVF conference on computer vision and pattern recognition*, 2019, pp. 4561–4570.
- [13] Yi Li, Gu Wang, Xiangyang Ji, Yu Xiang, and Dieter Fox, “Deepim: Deep iterative matching for 6d pose estimation,” in *Proceedings of the European Conference on Computer Vision (ECCV)*, 2018, pp. 683–698.
- [14] Bowen Wen, Wei Yang, Jan Kautz, and Stan Birchfield, “Foundationpose: Unified 6d pose estimation and tracking of novel objects,” in *Proceedings of the IEEE/CVF Conference on Computer Vision and Pattern Recognition*, 2024, pp. 17868–17879.
- [15] Pengshuai Yin, Jiayong Ye, Guoshen Lin, and Qingyao Wu, “Graph neural network for 6d object pose estimation,” *Knowledge-Based Systems*, vol. 218, pp. 106839, 2021.
- [16] Ruyi Lian and Haibin Ling, “Checkerpose: Progressive dense keypoint localization for object pose estimation with graph neural network,” in *Proceedings of the IEEE/CVF International Conference on Computer Vision*, 2023, pp. 14022–14033.
- [17] Alireza Rezaeadeh, Snehal Dikhale, Soshi Iba, and Nawid Jamali, “Hierarchical graph neural networks for proprioceptive 6d pose estimation of in-hand objects,” in *2023 IEEE International Conference on Robotics and Automation (ICRA)*, 2023, pp. 2884–2890.
- [18] Kaiming He, Xiangyu Zhang, Shaoqing Ren, and Jian Sun, “Deep residual learning for image recognition,” in *Proceedings of the IEEE conference on computer vision and pattern recognition*, 2016, pp. 770–778.
- [19] PC McCarthy, JE Sayre, and BLR Shawyer, “Generalized legendre polynomials,” *Journal of mathematical analysis and applications*, vol. 177, no. 2, pp. 530–537, 1993.
- [20] William H Press, *Numerical recipes 3rd edition: The art of scientific computing*, Cambridge university press, 2007.
- [21] Ashish Vaswani, Noam Shazeer, Niki Parmar, Jakob Uszkoreit, Llion Jones, Aidan N Gomez, Łukasz Kaiser, and Illia Polosukhin, “Attention is all you need,” *Advances in neural information processing systems*, vol. 30, 2017.
- [22] Andre Martins and Ramon Astudillo, “From softmax to sparsemax: A sparse model of attention and multi-label classification,” in *International conference on machine learning*. PMLR, 2016, pp. 1614–1623.
- [23] Chen Wang, Danfei Xu, Yuke Zhu, Roberto Martín-Martín, Cewu Lu, Li Fei-Fei, and Silvio Savarese, “Densefusion: 6d object pose estimation by iterative dense fusion,” in *Proceedings of the IEEE/CVF conference on computer vision and pattern recognition*, 2019, pp. 3343–3352.
- [24] Xinke Deng, Arsalan Mousavian, Yu Xiang, Fei Xia, Timothy Bretl, and Dieter Fox, “Poserbpf: A rao–blackwellized particle filter for 6-d object pose tracking,” *IEEE Transactions on Robotics*, vol. 37, no. 5, pp. 1328–1342, 2021.
- [25] Heng Zhao, Shenxing Wei, Dahu Shi, Wenming Tan, Zheyang Li, Ye Ren, Xing Wei, Yi Yang, and Shiliang Pu, “Learning symmetry-aware geometry correspondences for 6d object pose estimation,” in *Proceedings of the IEEE/CVF International Conference on Computer Vision*, 2023, pp. 14045–14054.
- [26] Wei Chen, Xi Jia, Hyung Jin Chang, Jinming Duan, and Ales Leonardis, “G2l-net: Global to local network for real-time 6d pose estimation with embedding vector features,” in *Proceedings of the IEEE/CVF conference on computer vision and pattern recognition*, 2020, pp. 4233–4242.
- [27] Xiao Lin, Deming Wang, Guangliang Zhou, Chengju Liu, and Qijun Chen, “Transpose: 6d object pose estimation with geometry-aware transformer,” *Neurocomputing*, vol. 589, pp. 127652, 2024.